Simple synthesis of silver nanocluster composites AgNCs@PE-g-PAA by irradiation method and fluorescence detection of Cr^{3+}

Fei Han[1,2], Wen-Rui Wang[1,2], Dan-Yi Li[1,2], Mou-Hua Wang[1,2], Ji-Hao Li[1,2,3,*], Lin-Fan Li[1,2,3,*]

[1] Shanghai Institute of Applied Physics, Chinese Academy of Sciences, Shanghai 201800, China

[2] University of Chinese Academy of Sciences, Beijing 100049, China

[3] Wuwei Institute of New Energy, Wuwei 733000, China

[*]Corresponding author, lilinfan@sinap.ac.cn (Linfan Li); lijihao@sinap.ac.cn (Jihao Li)

This work was supported by the Gansu Natural Science Foundation (Nos. 20JR10RA778 and 20JR10RA777).

ABSTRACT： Silver nanoclusters (AgNCs) are a new type of nanomaterials with similar properties to molecules and unique applications. The applications of AgNCs can be significantly expanded by combining them with different matrix materials to obtain AgNC composites. Using irradiation techniques, we developed a simple two-step method for preparing silver nanocluster composites. First, polyacrylic acid (PAA) chains were grafted onto the surface of a PE film as templates (PE-g-PAA). Subsequently, silver ions were reduced in situ on the surface of the template material to obtain the AgNC composites (AgNCs@PE-g-PAA). The degree of AgNC loading on the composite film was easily controlled by adjusting the reaction conditions. The loaded AgNCs were anchored to the carboxyl groups of the PAA and wrapped in the graft chain. The particle size of the AgNCs was only 4.38±0.85 nm, with a very uniform particle size distribution. The AgNCs@PE-g-PAA exhibited fluorescence characteristics derived from the AgNCs. The fluorescence of the AgNCs@PE-g-PAA was easily quenched by Cr^{3+} ions. The composite can be used as a fluorescence test paper to realize visual detection of Cr^{3+}.

KEYWORDS: Silver nanoclusters, Irradiation grafting, Irradiation reduction, In situ preparation, Fluorescence detection

1 INTRODUCTION

Metal nanoclusters (MNCs), especially Au nanoclusters (AuNCs) and Ag nanoclusters (AgNCs), are a new type of nanomaterials and are widely used in various fields[1-4]. Because of their extremely small size, MNCs exhibit unique properties that differ from those of metal nanoparticles (MNPs). The size of the MNCs is similar to the Fermi wavelength of electrons, which causes the MNCs to have discrete energy levels and exhibit molecular properties [5]. A unique property of MNCs, especially silver nanoclusters, is photoluminescence [5]. AgNCs have good photostability, low toxicity, and biocompatibility [6], and have been widely studied and applied [7, 8]. Compared with semiconductor quantum dots or organic dyes, AgNCs are characterized by better photostability, lower toxicity, and a larger Stokes shift [9]. The unique photoluminescence properties of silver nanoclusters provide a good platform for constructing luminescent probes for biological imaging and sensing applications [10-12].

Owing to their excellent performance, the fabrication of AgNCs for widespread use in various fields is of practical significance. Simple methods of obtaining AgNCs are required to solve the above problems. Currently, the synthesis of AgNCs is primarily based on traditional chemical reduction [13]. With the further exploration of AgNCs, ultraviolet reduction [14] and ultrasonic reduction [15] have also been exploited in the synthesis of AgNCs. These synthesis methods typically employ a range of reducing agents, including sodium borohydride, or energy-intensive complex instruments, to reduce Ag^+ ions to AgNCs in the presence of templates. This often leads to difficulties in the practical applications of AgNCs. Therefore, the development of a simple preparation method is required for promoting the practical application of AgNCs. Due to the reducing atmosphere from the interaction between water molecules and γ-rays [16], the strong penetrating ability of γ-rays [17], and the spontaneous generation of γ-rays by radionuclides [18], AgNCs can be synthesized by radiometric reduction. The principle of irradiation reduction has been extensively studied. Under the action of γ-rays, water molecules are ionized to produce a series of active substances, including hydrated electrons with strong reducibility [16]. Ag^+ ions are reduced to Ag atoms by hydrated electrons to form AgNCs under the action of the templates [16]. We successfully prepared an aqueous silver nanocluster solution by radiation reduction [19]. Compared with traditional methods, irradiation reduction synthesis requires simpler conditions, the reaction process is easy to control, and it is easier to achieve industrialization. Based on the above discussion, radiometric reduction may be an excellent method for the practical synthesis of AgNCs.

Compared to silver nanoparticles (AgNPs), AgNCs have unique photoluminescence capabilities [20]. Thus, AgNCs as have been used as fluorescent sensors [21, 22] for detecting various chemical substances such as metal ions [23], organic reagents [24], and biological molecules [21]. Dong and Wei et al. prepared DNA-AgNCs using DNA as a template for the detection of adenosine triphosphate (ATP) [25]. Dong et al. synthesized DNA-stabilized AgNCs for the quantitative detection of mercury ions [26]. However, most of these studies used only AgNC solutions for fluorescence detection. In solution, AgNCs tend to aggregate and lose their fluorescence characteristics because of their small size and high activity [20]. An effective approach is to anchor the AgNCs to the surfaces of solid materials. Currently, many solid materials are used to load AgNCs and the resulting compliant materials are used in various fields. Yang et al. introduced AgNCs into DNA hydrogels and obtained multifunctional hydrogels with both fluorescence and antibacterial abilities [27], while Yang et al. introduced DNA-stabilized AgNCs into graphene materials to detect tumor markers [28]. Irradiation grafting is a simple and universal way to obtain grafted polymer materials by free radical polymerization induced by γ-rays on the surface of matrix materials [29-31]. Because γ-rays are non-selective, irradiation grafting is highly versatile and expansible. The template monomer can be grafted onto the ligand polymer using an irradiation grafting technique to obtain a solid template. Silver nanoclusters were synthesized in situ on a matrix using anchor groups on a solid template enabling the simple and effective preparation of silver nanocluster composites in this study. This simple and general synthesis route has strong expansibility, which is beneficial for promoting the practical applications of Ag nanoclusters and broadening their application scope.

Trivalent chromium (Cr^{3+}) is widely present in wastewater from tanneries, electroplating, dyeing, and other industries [32]. Cr^{3+} can exert serious effects on the cell structure by binding to DNA and can cause great harm to the human body [33, 34]. Therefore, Cr^{3+} is considered an environmental pollutant that is harmful to humans.

Currently, Cr ion detection often relies on complex instruments and laboratory environments [35, 36]. Therefore, fluorescence detection based on the fluorescence characteristics of AgNCs is a simple and effective method of detecting Cr^{3+} ions. At present, the AgNCs used for Cr^{3+} detection are solution systems [37]. Although this method can achieve high sensitivity, AgNCs in solution are inconvenient for actual production processes. Therefore, detecting the fluorescence of Cr^{3+} using solid materials such as test paper is comparatively simpler and more convenient.

Herein, using polyacrylic acid (PAA) as a template, composites loaded with AgNCs are obtained via a two-step irradiation process. In the first step, the template monomer, acrylic acid (AA), is grafted onto the PE matrix material by irradiation grafting, and a PE film grafted with AA (PE-g-PAA) is obtained. In the second step, through irradiation reduction, Ag^{+} ions are reduced in situ on the PE-g-PAA film to obtain film materials loaded with AgNCs (AgNCs@PE-g-PAA). The degree of nanocluster loading in the AgNCs@PE-g-PAA is effectively regulated by simply controlling the reaction conditions. The bonded PAA molecular chains can act as a template to prevent agglomeration of the AgNCs. The loaded AgNCs also enable the formation of photoluminescent AgNCs@PE-g-PAA film materials. The prepared AgNCs@PE-g-PAA film exhibits obvious fluorescence quenching of Cr^{3+} and can be used as a fluorescence detection paper for Cr^{3+}. Furthermore, the mechanism of fluorescence quenching of AgNCs by Cr^{3+}, which is a static quenching mechanism, is explored.

2 EXPERIMENTAL SECTION

2.1 Materials. Acrylic acid (AA), ferric chloride, acetone, silver nitrate, and isopropyl alcohol were purchased from Sinopharm Chemical Reagent Co., Ltd. (Shanghai, China). Chromium nitrate, aluminum nitrate, iron nitrate, copper nitrate, and mercury nitrate were purchased from Sinopharm Chemical Reagent Co., Ltd. (Shanghai, China). All chemicals and solvents used were analytical reagents (AR). All chemicals and solvents were used as received, without further purification. PE film was used in this experiment. The water used in all experiments was purified using a Millipore system.

2.2 Instrumentation. Steady-state absorption measurements were performed on a HITACHI U-3900 UV-vis spectrophotometer by scanning in the range of 300–800 nm. The steady-state luminescence measurements were performed using a spectrofluorometer (FS5). The luminescence spectra were acquired using a quartz cuvette, with an integration time of 0.1 s. The excitation and emission slits were maintained at 3 nm. Infrared (IR) analysis was performed using an FTIR650 spectrophotometer over the range of 600–4000 cm^{-1} at a resolution of 2 cm^{-1}. For the lifetime measurements, the AgNCs were excited at 540 nm using an IBH-NanoLED source (N-340). The emissions were collected at a magic-angle polarization using a Hamamatsu MCP photomultiplier (Model R-3809U-50). Transmission electron microscopy (TEM) images were obtained using a JEM-3000F high-resolution transmission instrument operating at 200 kV. Thin TEM samples were prepared using the ultrathin frozen-section technique. For field-emission scanning electron microscopy (FESEM) imaging, a JSM-6700F instrument was used to capture the SEM images at an accelerating voltage of 10–15 kV. The energy dispersive X-ray spectroscopy (EDS) images were collected at an accelerating voltage of 15 kV. Valence analysis of the elements on the film surface was performed by X-ray photoelectron spectroscopy (XPS; SCIENTIFICESCALAB 250Xi) and fitted using software. To study the thermal properties of the material, a TG 209F4 instrument was

used to test the thermogravimetric behavior of the material, and a METTLER TOLEDO DSC3 apparatus was used to determine the glass transition temperature and melting point of the material. The static contact angles of the materials were measured using a THETA Optical tensiometer. The fluorescence of all materials was observed using a ZF-1 UV analyzer at 365 nm.

2.3 Synthesis of PE-g-PAA. The PE-g-PAA film was synthesized via irradiation grafting. First, 0.72 g of acrylic acid was dissolved in acetone (20 mL) and stirred for 1 h until the solution was thoroughly mixed. Subsequently, 0.0072 g of ferric chloride was added and stirred until the solution was fully mixed. At the same time, the commercial PE film was cleaned with deionized water and dried at 60 ℃in an oven. The pretreated PE film was then immersed in the prepared acrylic acid–ferric chloride–acetone solution. Subsequently, the solution was sparged with N_2 for 15 min and then irradiated at an absorbed dose of 20 kGy through Co_{60}. The total synthesis was conducted at room temperature. After irradiation, the graft film was ultrasonically cleaned with deionized water for 1 h, during which time the deionized water was replaced three times. The films were dried in an oven at 60 °C for 24 h and weighed again. The degree of grafting (DG) was determined as the percentage increase in the film weight, according to Eq. (1):

where, W_g and W_0 are the weights of the grafted and ungrafted films, respectively.

2.4 Synthesis of AgNCs@PE-g-PAA. The AgNCs@PE-g-PAA film was synthesized by irradiation reduction. First, 0.34 g of silver nitrate and 0.6 g of isopropyl alcohol were combined in deionized water and stirred for 30 min until they were well mixed. Thereafter, the previously prepared PE-g-PAA graft film was immersed in a silver nitrate–isopropyl alcohol–aqueous solution and incubated for 2 h until the silver particles combined with the film material. Subsequently, the solution was sparged with N_2 for 15 min and then irradiated at an absorbed dose of 600 Gy through Co_{60}. The total synthesis was conducted at room temperature. After irradiation, the loaded film was ultrasonically cleaned with deionized water for 6 min, during which the deionized water was replaced twice. The film was left at room temperature for 24 h, dried, and weighed. The degree of loading (DL) was determined as the percentage increase in the film weight according to Eq. (2):

where, W_g and W_0 are the weights of the grafted and ungrafted films, respectively.

Finally, the loaded AgNCs@PE-g-PAA film was stored in a refrigerator at 4 ℃ for subsequent testing.

2.5 Detection of Cr^{3+}. A stock solution of Cr^{3+} was prepared by dissolving a certain amount of chromium nitrate in deionized water. The stock solution of Cr^{3+} was diluted to obtain standard working solutions of different concentrations by adding deionized water. The AgNCs@PE-g-PAA film was immersed in the Cr^{3+} solution of the corresponding concentration and incubated at room temperature for 6 h. The film material was removed and dried at room temperature for analysis by fluorescence spectroscopy.

3 RESULTS AND DISCUSSION

Irradiation techniques such as irradiation grafting and irradiation reduction are simple and effective methods of modifying polymer composite materials[38] and reducing metal ions[39]. As the coordination site for silver nanoclusters, a PAA chain was first grafted onto a commercial PE film by irradiation grafting, and the Ag^+ ions were then reduced in situ to silver nanoclusters (AgNCs) by irradiation reduction to

obtain a composite film (AgNCs@PE-g-PAA) loaded with silver nanoclusters. The preparation of the AgNCs@PE-g-PAA is shown in Scheme 1. The addition of PAA can provide reliable binding sites for the silver nanoclusters, enabling stable loading of the silver nanoclusters. The irradiation technique is not dependent on specific functional groups or reagents and has strong universality. The synthesis of AgNCs@PE-g-PAA is flexible and extensible.

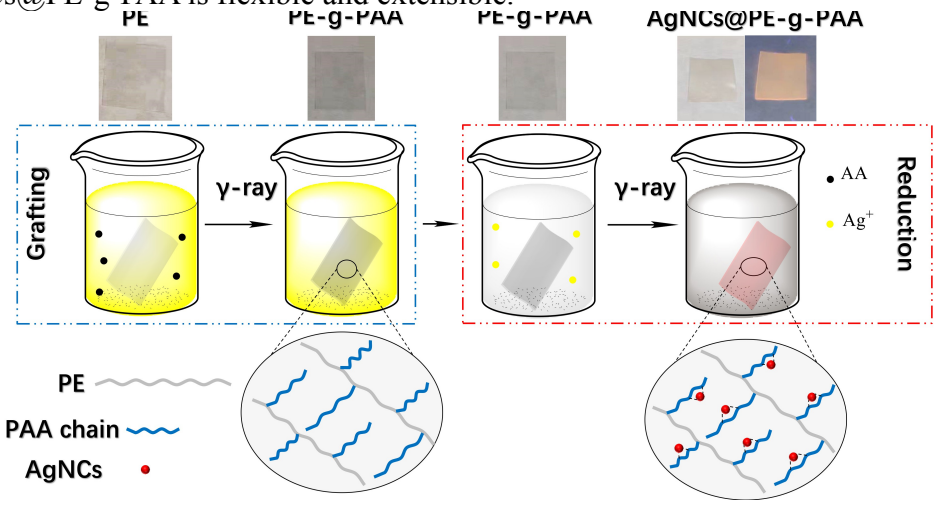

Scheme 1. Preparation of AgNCs@PE-g-PAA.

3.1 Preparation of AgNCs@PE-g-PAA. It is well known that AgNCs are very small in size and thus have very high activity. Without the protection of templates or stabilizers, AgNCs spontaneously aggregate to form more stable silver nanoparticles (AgNPs), which is not conducive to the practical application of AgNCs[20]. Typically, a series of templates or stabilizers containing O [15], N [40], and S [41] is used in the synthesis of AgNCs to prevent their aggregation into AgNPs. Here, the PAA chains grafted onto PE films can be used as sites to stabilize the AgNCs.

To confirm the formation of the AgNCs@PE-g-PAA film, Fourier-transform infrared spectroscopy (FT-IR) measurements were performed; the results are presented in Fig. 1(a). The characteristic peak at 1730 cm^{-1} corresponds to the carboxyl group of the graft monomer acrylic acid (AA), indicating the successful synthesis of PE-g-PAA. Note that the irradiation grafting mechanism is a traditional free radical polymerization mechanism[42], which is a mature and efficient technique[43]. Therefore, the degree of grafting of PE-g-PAA can be controlled by controlling the reaction conditions, such as the absorption dose, AA concentration, and polymerization inhibitor content, thereby affecting the loading process of the AgNCs. By controlling the above factors, the graft polymerization was effectively controlled, and the degree of grafting of the PE-g-PAA film was controlled from 0% to 170% (Fig. S1).

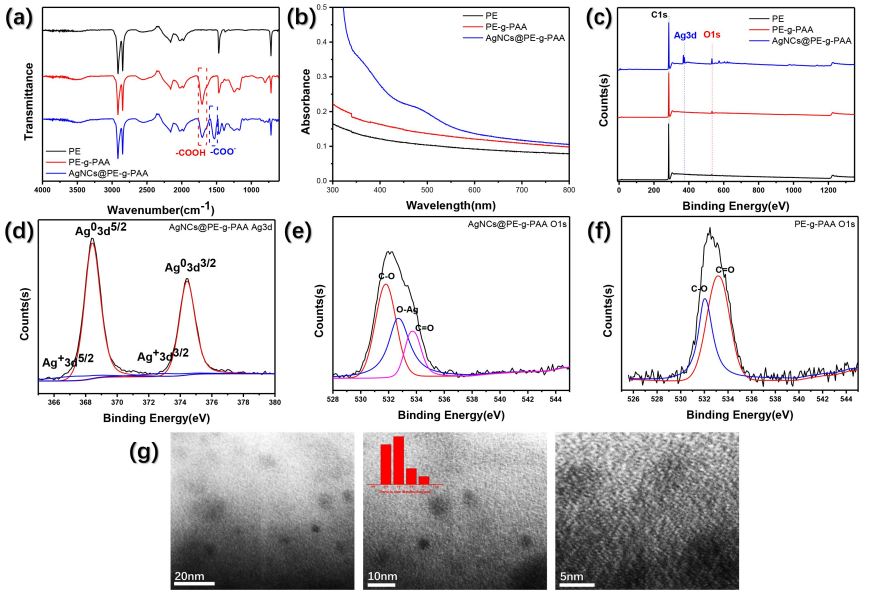

Fig. 1. (Color online) (a) Fourier-transform infrared spectra of PE, PE-g-PAA, and AgNCs@PE-g-PAA; (b) UV-vis spectrum of AgNCs@PE-g-PAA; (c) XPS profile of AgNCs@PE-g-PAA; (d) Ag3d XPS profile of AgNCs@PE-g-PAA; (e) O1s XPS profile of AgNCs@PE-g-PAA; (f) O1s XPS profile of PE-g-PAA; (g) TEM image of AgNCs@PE-g-PAA (inset: particle size distribution).

A suitable solid template is favorable for loading and stabilizing the AgNCs. The PE-g-PAA film can play a role in the in-situ synthesis and long-term protection of AgNCs. The UV-vis spectra (Fig. 1(b)) of PE and PE-g-PAA have no obvious absorption peaks in the range of 300–800 nm. In contrast, the prepared AgNCs@PE-g-PAA film exhibited a weak absorption peak at 500 nm (Fig. 1(b)), which corresponds to the absorption peak of the AgNCs[44]. AgNCs@PE-g-PAA produced fluorescence emission at a wavelength of 650 nm under visible-light excitation at 540 nm (Fig. S4(a)), and also produced visible fluorescence under irradiation with 365 nm UV light (Scheme 1), which is attributed to the photoluminescence of the AgNCs. XPS was used to verify the formation of the AgNCs (Fig. 1(c)). The peaks at 368 eV and 374 eV in the Ag3d spectrogram reveal the formation of Ag^0 (Fig. 1(d)). In summary, these phenomena indicate the successful synthesis of AgNCs.

Furthermore, the interaction between the AgNCs and the PE-g-PAA template was investigated. As the AgNCs bind with carboxyl groups, the carboxyl group on the graft chain ionizes and forms a carboxylic acid group that participates in the coordination process with the AgNCs, resulting in the characteristic peak of the carboxylate group of PAA at 1550 cm^{-1} (Fig. 1(a)). By analyzing the chemical state of oxygen in the material, it was found that after loading the AgNCs, O on the surface of the film material exhibited a new peak (Fig. 1(e)) that did not exist in the spectrum of PE-g-PAA (Fig. 1(f)). This may be related to the coordination between the O atoms in the carboxyl group and Ag atoms in the AgNCs, leading to a change in the chemical state of O. Therefore, the interaction between the carboxyl group and AgNCs plays a key role in stabilizing the AgNCs. When the degree of PE-g-PAA grafting was 0%, no AgNCs were generated in the material (Fig. S2). This phenomenon also supports the important role of PAA in stabilizing the AgNCs.

Irradiation reduction is similar to irradiation grafting and has strong universality[17]. The degree of loading of AgNCs@PE-g-PAA could also be controlled

by controlling the number of anchor sites on the film surface and the degree of reduction of Ag^+ ions, in a similar manner to controlling the degree of grafting of PE-g-PAA. By controlling the degree of grafting, Ag^+ ion concentration, and the absorbed dose of PE-g-PAA, the degree of loading of AgNCs@PE-g-PAA was easily controlled between 0% and 35% (Fig. S2).

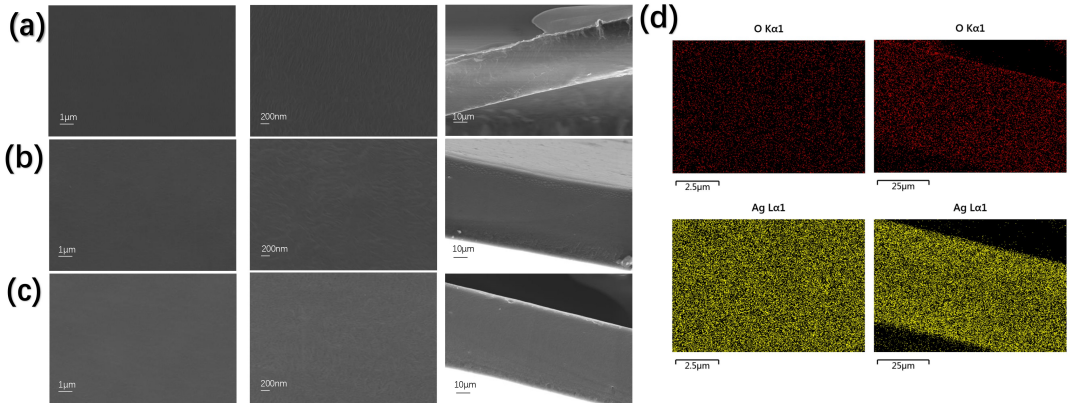

Fig. 2 (Color online) (a) SEM images of PE surface and cross-section; (b) SEM images of PE-g-PAA surface and cross-section; (c) SEM images of AgNCs@PE-g-PAA surface and cross-section; (d) EDS image of surface and cross-section of AgNCs@PE-g-PAA.

The morphology and distribution of the AgNCs in the AgNCs@PE-g-PAA films were also studied. As shown in Fig. 1(g), the prepared AgNCs were wrapped in the AgNCs@PE-g-PAA film and exhibited a spherical shape with an average particle size of 4.38±0.85 nm. The uniform distribution of AgNCs on the film material was observed more clearly through elemental analysis at the nanoscale (Fig. S3). The morphological changes in the surface and cross-sectional profiles of the film materials were observed by SEM at a larger scale. As shown in Fig. 2(a), the ordinary commercial PE film has a typical planar structure with a substantial nonporous cross-sectional structure. After grafting PAA and loading the AgNCs, the film surface and cross-sectional morphology (Fig. 2(b), Fig. 2(c)) did not change significantly. The EDS images (Fig. 2(d)) show that O was evenly distributed on the surface of the PE film, indicating that the grafted chain PAA was evenly distributed on the PE film. This is conducive to the uniform loading of the AgNCs. As expected, Ag was evenly distributed on the surface of the film (Fig. 2(d)), indicating that the AgNCs@PE-g-PAA achieved uniform loading of the AgNCs. Interestingly, the EDS map (Fig. 2(d)) of the cross-section of the AgNCs@PE-g-PAA film shows that O and Ag were distributed throughout the cross-section, indicating that AA grafting and AgNC loading not only occur on the surface of the film, but also on the interior of the film. This may be due to the swelling behavior of PE during the reaction. As a good solvent for PE, acetone does not dissolve PE at room temperature, but causes it to swell. Thus, AA molecules could penetrate the PE film, resulting in a graft reaction in the interior of the PE film and the formation of PAA molecular chains in the film. Owing to the good hydrophilicity of the graft-chain PAA, the template PE-g-PAA film will exhibit similar swelling behavior in aqueous solution, leading to the reduction of silver ions in the film. This is conducive to the loading of AgNCs inside the film. Therefore, the template chain PAA and AgNCs were stably distributed throughout the material (Fig. 2(d)).

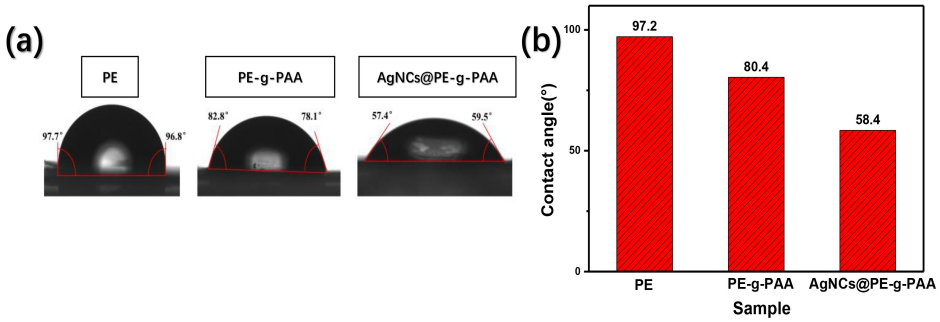

Fig. 3. (Color online) (a) Photographs of water droplets on the film surface (from left to right: PE, PE-g-PAA,AgNCs@PE-g-PAA); (b) changes in contact angle of film material.

The morphology of the film did not change during the synthesis of AgNCs@PE-g-PAA, indicating that the synthesis process did not cause serious damage to the matrix. This improves the universality of the synthesis method. The matrix material used in this study was a commercial PE film. The PE film comprises a nonpolar -CH_2-CH_2- structure. As shown in Fig. 3(a) and Fig. 3(b), the contact angle of the commercial PE film is 97°, indicating that the material is hydrophobic. After the grafting of PAA, the contact angle of PE-g-PAA decreased to 80° (Fig. 3B(b)) because of the strong polarity of the carboxyl group of PAA, and the material became hydrophilic. This is conducive to the subsequent adsorption of Ag^+ ions from the aqueous solution to achieve the loading of AgNCs. After loading the AgNCs, the contact angle of the AgNCs@PE-g-PAA film decreased further to 58° (Fig. 3(b)). Owing to the combination of AgNCs and the carboxyl groups on the PAA chain, the polarity of the material increased, and the material became more hydrophilic[45]. In addition, the AgNCs@PE-g-PAA film could be used to detect metal ions in aqueous solutions.

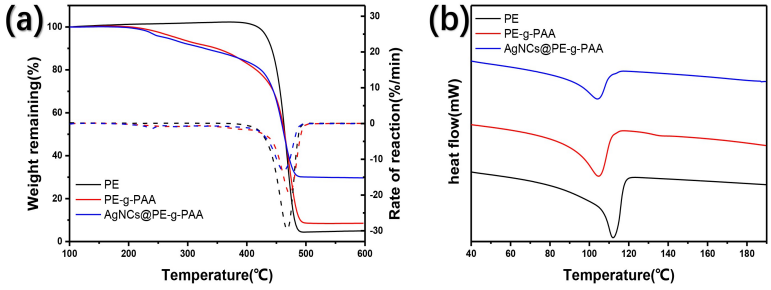

Fig. 4. (Color online) (a) TGA thermograms and corresponding rates for PE, PE-g-PAA, AgNCs@PE-g-PAA; (b) DSC thermograms of PE, PE-g-PAA and AgNCs@PE-g-PAA.

To further study the changes in the material during the synthesis process, TG and DSC were used to analyze the material. The thermogravimetric curve (Fig. 4(a)) of the PE film shows a single weight loss at 390–500 ℃ due to the thermal decomposition of the polymer backbone. After grafting PAA, along with breaking of the polymer backbone, the PE-g-PAA film showed a mass loss at 170 ℃ This part of the thermogravimetric process is caused by the dehydration of adjacent carboxyl groups to form anhydride[29]. The thermal decomposition curve (Fig. 4(a)) of the AgNCs@PE-g-PAA film was almost the same as that of the PE-g-PAA film. The temperature corresponding to the maximum thermal decomposition rate was considered the maximum thermal decomposition temperature of the material. The

maximum thermal decomposition temperature of PE was 468.8 ℃(Fig. 4(a)), and the film was almost completely decomposed. The maximum thermal decomposition temperature of the PE-g-PAA film was 472.5 ℃ (Fig. 4(a)), and the final thermal decomposition was almost complete. The maximum thermal decomposition temperature of the AgNCs@PE-g-PAA film was 462.2 ℃ (Fig. 4(a)), and the final weight loss was ~70%. The mass percentage difference between the AgNCs@PE-g-PAA film and PE-g-PAA was consistent with the degree of loading of AgNCs@PE-g-PAA. The DSC scan (Fig. 4(b)) shows a slight decrease in the melting point of the film after grafting with AA, whereas the melting point of the film did not change after further loading of the silver nanoclusters. More comprehensively, there was no obvious damage to the matrix material during the synthesis. In addition, with the grafting of AA and the loading of AgNCs, the melting enthalpy of the PE film decreased gradually (Fig. 4(b)), indicating that its crystal region was destroyed by irradiation; however, this did not affect its application as a metal ion sensor.

3.2 Fluorescence of AgNCs@PE-g-PAA. Compared to AgNPs with larger particle sizes, the bright fluorescence emission was unique to the AgNCs. Under UV light at 365 nm, AgNCs@PE-g-PAA produced bright, red fluorescence emission (Scheme 1). Upon excitation at 540 nm, AgNCs@PE-g-PAA exhibited the strongest fluorescence at 650 nm (Fig. S4(a)). Compared with conventional organic dyes, silver nanoclusters have a larger Stokes shift, which is beneficial for improving the identification efficiency[15]. Moreover, because the excitation wavelength of the AgNCs is within the range of visible light, AgNCs@PE-g-PAA could still be excited under natural light, which was light red (Scheme 1). This facilitates the visual detection of ions by the film materials under natural light. The quantum yield of AgNCs@PE-g-PAA was 0.125, which is close to that of AgNCs reported in another study[46]. From the excited-state decay profile (Fig. S4(c)) of AgNCs@PE-g-PAA, the fluorescence lifetime of the AgNCs was determined as1.43 ns. The nanosecond fluorescence lifetime of the AgNCs indicates that their photoluminescence is fluorescence emission rather than phosphorescent emission, and the excited electrons directly emit fluorescence by returning to the ground state without passing through the triplet state[15]. Notably, the fluorescence emission of the synthesized AgNCs@PE-g-PAA films was dependent on the excitation wavelength. Under excitation at 480 nm, the AgN@g-AA film presented two fluorescence peaks with maxima at 640 nm and 730 nm, where the fluorescence peak at 730 nm was stronger (Fig. S4(b)). With increasing excitation wavelength, the long-wavelength emission peak gradually weakened, the short-wavelength emission peak gradually strengthened, and the spectrum gradually resolved to only the short-wavelength emission peak (Fig. S4(b)). With an increase in the excitation wavelength, the maximum of the short-wavelength emission peak was gradually red-shifted, and its intensity first increased. When the excitation wavelength was greater than 530 nm, the fluorescence intensity decreased slightly (Fig. S4(b)). This indicates that the AgNC fluorescence emission on the AgNCs@PE-g-PAA film was also produced by AgNCs containing different numbers of silver atoms. The failure to form monodisperse AgNCs may be due to the use of a polymer template, which hindered the formation of a fixed structure. This is consistent with the performance of AgNCs formed using other polymer templates[44].

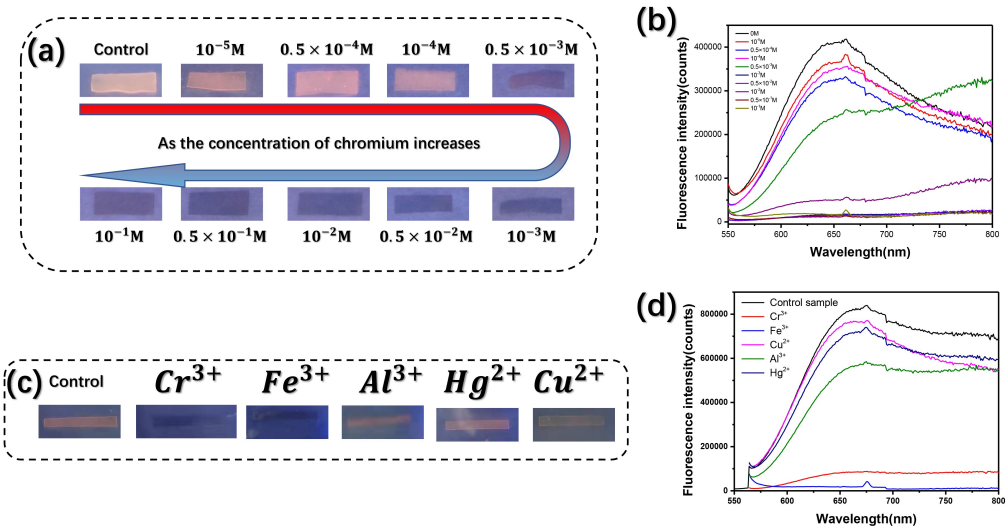

Fig. 5. (a) Fluorescence of AgNCs@PE-g-PAA at different Cr^{3+} concentrations; (b) fluorescence spectra of AgNCs@PE-g-PAA at different Cr^{3+} concentrations; (c) fluorescence of AgNCs@PE-g-PAA at different metal ion concentrations of 10^{-3} M; (d) fluorescence spectra of AgNCs@PE-g-PAA at metal ion concentration of 10^{-3} M.

3.3 Detection of Cr^{3+}. Trivalent chromium (Cr^{3+}) is an important environmental pollutant, where these ions are widely used in industry and agriculture[47]. Therefore, it is important to develop a low-cost method of detecting Cr^{3+}. Based on the bright fluorescence of the AgNCs, the AgNCs@PE-g-PAA film can be used as a fluorescent test paper for the detection of metal ions. When the prepared AgNCs@PE-g-PAA film was exposed to Cr^{3+}, the fluorescence of the film was quenched (Fig. 5(a)). This indicates that AgNCs@PE-g-PAA can be used as a fluorescent test paper for detecting Cr^{3+}. Firstly, the degree of fluorescence quenching AgNCs@PE-g-PAA depended on the concentration of Cr^{3+} (Fig. 5(a), Fig. 5(b)). When the concentration of Cr^{3+} was low, the fluorescence of AgNCs@PE-g-PAA did not change significantly, and the fluorescence intensity at 650 nm did not decrease significantly (Fig. 5(a), Fig. 5(b)). When the Cr^{3+}concentration was greater than 10^{-4} M, the fluorescence intensity of AgNCs@PE-g-PAA decreased significantly (Fig. 5(b)). Notably, the fluorescence quenching time of AgNCs@PE-g-PAA differed for different concentrations of Cr^{3+}. At higher concentrations of Cr^{3+}, the fluorescence quenching of AgNCs@PE-g-PAA occurred more rapidly (Fig. S5). Even at low Cr^{3+} concentrations, the synthesized AgNCs@PE-g-PAA film could detect Cr^{3+} within a response time of 3 h (Fig. S5). To further evaluate the selectivity of AgNCs@PE-g-PAA for Cr^{3+}, we attempted to detect several other common metal ions as controls, including Fe^{3+}, Cu^{2+}, Al^{3+}, and Hg^{2+}, at the Cr^{3+} response concentrations. Under UV light at 365 nm, the fluorescence of the AgNCs@PE-g-PAA films exposed only to Cr^{3+} and Fe^{3+} ions disappeared, while the other films retained bright fluorescence (Fig. 5(c)). Compared to the control sample, the fluorescence intensity of the film materials exposed to Fe^{3+} and Cr^{3+} decreased by an order of magnitude (Fig. 5(d)). The fluorescence intensity of the film materials exposed to Cr^{3+} decreased significantly (Fig. 5(d)). In natural light, AgNCs@PE-g-

PAA appeared yellow when exposed to iron ions and blue when exposed to chromium ions (Fig. S6). Therefore, AgNCs@PE-g-PAA exhibited good selectivity for Cr^{3+} through color change and fluorescence quenching. The reliability of AgNCs@PE-g-PAA was also further tested by simply using domestic water instead of deionized water. AgNCs@PE-g-PAA could still detect Cr^{3+} in complex ionic environments (Fig. S7). As shown in Table 1, compared with other detection methods such as AAS and ICP-MS, there is still a large gap in the detection performance of AgNCs@PE-g-PAA. However, these traditional methods often require complex pre-treatment processes and laboratory conditions. The low requirements for the original sample and testing environment are advantages of AgNCs@PE-g-PAA for ion detection. Therefore, it was confirmed that AgNCs@PE-g-PAA has good selectivity for Cr^{3+}, ensuring that it can be used as a test paper for the detection of Cr^{3+}.

Table 1 Comparison of different Cr^{3+} detection methods

Method	Test substance	Detection limit	References
Resonance Rayleigh scattering	Cr^{3+}	1.0pM	[48]
CEC -ICPMS	CrO_4^{2-}–Cr^{3+}	＜0.02μM	[49]
LA-ICPMS	Cr^{3+}	0.02mM	[50]
Ion interaction chromatography	Cr^{3+}	0.4μM	[51]
Electrochemistry	Cr^{3+}	4.1nM	[35]
Atomic absorption spectrometry	Cr^{3+}	3.8 nM	[52]
AgNCs@PE-g-PAA	Cr^{3+}	1mM	This work

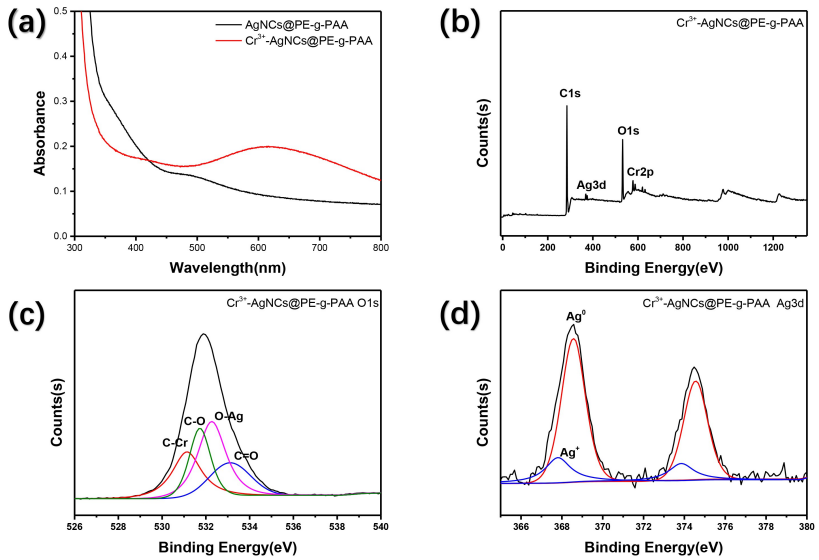

Fig. 6. (Color online) (a) UV-vis spectra before and after exposure to Cr^{3+}; (b) XPS profile of AgNCs@PE-g-PAA exposed to Cr^{3+}; (c) O1s XPS profile of AgNCs@PE-g-PAA exposed to Cr^{3+}; (d) Ag3d XPS profile of AgNCs@PE-g-PAA exposed to Cr^{3+}.

The mechanism underlying the ability of AgNCs@PE-g-PAA to detect Cr^{3+} was studied. For the entire detection system, dry solid film materials were used for testing

using fluorescence spectroscopy. In contrast with other currently used AgNC solutions, the AgNCs in the AgNCs@PE-g-PAA films were riveted on the surface of the film materials, making it difficult for them to come into contact with each other. Therefore, it is difficult to quench the fluorescence of AgNCs by dynamic quenching. In the UV-vis spectra (Fig. 6(a)), the absorption peak of the AgNCs at 500 nm disappeared after treatment with Cr^{3+}. This indicates that the introduction of Cr^{3+} causes the material to form a new complex that changes the light-absorption of the AgNCs. Based on the above analysis, the fluorescence quenching of AgNCs by Cr^{3+} occurs via a static quenching mechanism. It is well known that AgNCs@PE-g-PAA contains a large number of carboxyl groups, which have strong ability to coordinate on many metal ions and are often used to adsorb these metal ions[39]. Cr^{3+} ions in solution could also be captured and adsorbed by the carboxyl groups on the film materials. The XPS profile in Fig. 6(b) shows an intense absorption peak of Cr on the surface of the AgNCs@PE-g-PAA film (Cr^{3+}-AgNCs@PE-g-PAA) treated with Cr^{3+}. This indicates that the AgNCs@PE-g-PAA film was effective for adsorbing Cr^{3+} in solution. In addition, the carboxyl group in AgNCs@PE-g-PAA combined with the AgNCs and played a role in stabilizing the AgNCs. Therefore, when the AgNCs@PE-g-PAA film was immersed in the Cr^{3+} solution, Cr^{3+} was adsorbed on AgNCs@PE-g-PAA via the carboxyl groups and formed a non-fluorescent Cr^{3+}-AgNCs@PE-g-PAA complex, resulting in fluorescence quenching of the AgNCs. Compared with the chemical state of oxygen in PE-g-PAA (Fig. 1(f)), that of oxygen in AgNCs@PE-g-PAA was significantly different because of the coordination-stabilizing effect of the carboxyl group on the AgNCs (Fig. 1(e)). In turn, a new low-intensity peak appeared in the XPS O1s spectrogram (Fig. 6(c)) of the surface of the Cr^{3+}-AgNCs@PE-g-PAA film after the adsorption of Cr^{3+}, attributed to the combination of Cr and O atoms. After Cr^{3+} adsorption, the chemical state of Ag on the film material did not change, indicating that Cr^{3+} did not directly contact the AgNCs (Fig. 6(d)). This confirms that the formation of the Cr^{3+}-AgNCs@PE-g-PAA complex led to static fluorescence quenching of the AgNCs.

4 CONCLUSIONS

In summary, AgNCs@PE-g-PAA films were synthesized via a two-step process using irradiation. First, a poly(acrylic acid) (PAA) template was grafted onto PE by irradiation to obtain the PE-g-PAA template material. Second, Ag^{+} ions were reduced in situ on the PE-g-PAA film by irradiation to obtain AgNCs@PE-g-PAA. The degree of loading was controlled by varying the reaction conditions. The obtained AgNCs were extremely small and uniformly distributed on the film. AgNCs@PE-g-PAA exhibited a clear red fluorescence emission derived from the AgNCs. The fluorescence was quenched by Cr^{3+}, enabling the use of the system as a test paper for the detection of Cr^{3+}. Quenching occurred via the static mechanism. In conclusion, the irradiation technique can be used to load AgNCs onto solid materials in a simple and controllable manner, which improves the method of loading metal nanoclusters onto various matrix materials and expands the practical applications of metal nanoclusters.

Author contributions

All authors contributed to the study conception and design. Material preparation, data collection and analysis were performed by Fei Han, Wen-Rui Wang, Dan-Yi Li Mou-Hua Wang and Ji-Hao Li. The first draft of the manuscript was written by Fei Han under the guidance of Lin-Fan Li and all authors commented on previous versions of the manuscript. All authors read and approved the final manuscript.

Data Availability Statement

The data that support the findings of this study are openly available in Science Data Bank at https://www.doi.org/10.57760/sciencedb.j00186.00070 and http://resolve.pid21.cn/31253.11.sciencedb.j00186.0007.

References

[1] C.-C. Hsu, Y.-Y. Chao, S.-W. Wang, et al. Polyethylenimine-capped silver nanoclusters as fluorescent sensors for the rapid detection of ellagic acid in cosmetics. Talanta. 204. (2019). doi: 10.1016/j.talanta.2019.06.047

[2] L. Lu, X. An and W. Huang. Quantitative determination of calcium ions by means of enhanced fluorescence of silver nanocluster complex. Analytical Methods. 9. 1 (2017). doi: 10.1039/C6AY02477G

[3] Y. Tang, Y. Zhang, Y. Su, et al. Highly sensitive resonance light scattering bioassay for heparin based on polyethyleneimine-capped Ag nanoclusters. Talanta. 115. (2013). doi: 10.1016/j.talanta.2013.06.028

[4] J. Yang and R. C. Jin. New Advances in Atomically Precise Silver Nanoclusters. ACS Mater. Lett. 1. 4 (2019). doi: 10.1021/acsmaterialslett.9b00246

[5] L. Shang, S. J. Dong and G. U. Nienhaus. Ultra-small fluorescent metal nanoclusters: Synthesis and biological applications. Nano Today. 6. 4 (2011). doi: 10.1016/j.nantod.2011.06.004

[6] L. B. Zhang and E. K. Wang. Metal nanoclusters: New fluorescent probes for sensors and bioimaging. Nano Today. 9. 1 (2014). doi: 10.1016/j.nantod.2014.02.010

[7] H. Haidari, R. Bright, Z. Kopecki, et al. Polycationic Silver Nanoclusters Comprising Nanoreservoirs of Ag+ Ions with High Antimicrobial and Antibiofilm Activity. Acs Appl Mater Inter. 14, 1 (2021).doi: 10.1021/acsami.1c21657

[8] Y. M. Su, X. Y. Li, Z. Wang, et al. Structural rearrangement of Ag-60 nanocluster endowing different luminescence performances. J. Chem. Phys. 155. 23 (2021). doi: 10.1063/5.0070138

[9] S. Ghosh, U. Anand and S. Mukherjee. Luminescent Silver Nanoclusters Acting as a Label-Free Photoswitch in Metal Ion Sensing. Anal. Chem. 86. 6 (2014). doi: 10.1021/ac500122v

[10] H. Chen, Y. Li, Y. Song, et al. A sandwich-type electrochemical immunosensor based on spherical nucleic acids-templated Ag nanoclusters for ultrasensitive detection of tumor biomarker. Biosensors and Bioelectronics. 223. (2023). doi: 10.1016/j.bios.2022.115029

[11] Y. Jiang and P. Miao. DNA dumbbell and chameleon silver nanoclusters for mirna logic operations. Research. 2020. (2020). doi: 10.34133/2020/1091605

[12] K. Zheng, X. Yuan, N. Goswami, et al. Recent advances in the synthesis, characterization, and biomedical applications of ultrasmall thiolated silver nanoclusters. Rsc Adv. 4. 105 (2014). doi: 10.1039/c4ra12054j

[13] S. Choi, Y. Zhao and J. Yu. Generation of luminescent silver nanodots in the presence of amino silane and sodium polyacrylate. J. Photochem. Photobiol. A-Chem. 374. (2019). doi: 10.1016/j.jphotochem.2019.01.018

[14] Z. Shen, H. W. Duan and H. Frey. Water-soluble fluorescent Ag nanoclusters obtained from multiarm star poly(acrylic acid) as ″molecular hydrogel″ templates.

Advanced Materials. 19. 3 (2007). doi: 10.1002/adma.200601740
[15] H. X. Xu and K. S. Suslick. Sonochemical Synthesis of Highly Fluorescent Ag Nanoclusters. Acs Nano. 4. 6 (2010). doi: 10.1021/nn100987k
[16] J. V. Rojas and C. H. Castano. Radiation-assisted synthesis of iridium and rhodium nanoparticles supported on polyvinylpyrrolidone. J Radioanal Nucl Ch. 302. 1 (2014). doi: 10.1007/s10967-014-3291-y
[17] A. A. Zezin, D. I. Klimov, E. A. Zezina, et al. Controlled radiation-chemical synthesis of metal polymer nanocomposites in the films of interpolyelectrolyte complexes: Principles, prospects and implications. Radiat Phys Chem. 169. (2020). doi: 10.1016/j.radphyschem.2018.11.030
[18] S. Strohmaier and G. Zwierzchowski. Comparison of Co-60 and Ir-192 sources in HDR brachytherapy. J. Contemp. Brachytherapy. 3. 4 (2011). doi: 10.5114/jcb.2011.26471
[19] F. Han, J. Li, W. Wang, et al. Synthesis of silver nanoclusters by irradiation reduction and detection of Cr(3+) ions. Rsc Adv. 12. 51 (2022). doi: 10.1039/d2ra06536c
[20] I. Diez and R. H. A. Ras. Fluorescent silver nanoclusters. Nanoscale. 3. 5 (2011). doi: 10.1039/c1nr00006c
[21] L. S. Ardekani, T. T. Moghadam, P. W. Thulstrup, et al. Design and Fabrication of a Silver Nanocluster-Based Aptasensor for Lysozyme Detection. Plasmonics. 14. 6 (2019). doi: 10.1007/s11468-019-00954-5
[22] Q. L. Wen, J. Peng, A. Y. Liu, et al. DNA bioassays based on the fluorescence 'turn off' of silver nanocluster beacon. Luminescence. 35. 5 (2020). doi: 10.1002/bio.3775
[23] D. Li, B. Li, G. Lee, et al. Facile Synthesis of Fluorescent Silver Nanoclusters as Simultaneous Detection and Remediation for Hg2+. Bull. Korean Chem. Soc. 36. 6 (2015). doi: 10.1002/bkcs.10294
[24] J. H. Chen, X. Zhang, S. X. Cai, et al. A fluorescent aptasensor based on DNA-scaffolded silver-nanocluster for ochratoxin A detection. Biosens. Bioelectron. 57. (2014). doi: 10.1016/j.bios.2014.02.001
[25] Q. Qiu, R. R. Gao, A. M. Xie, et al. A ratiometric fluorescent sensor with different DNA-templated Ag NCs as signals for ATP detection. J. Photochem. Photobiol. A-Chem. 400. (2020). doi: 10.1016/j.jphotochem.2020.112725
[26] D. T. Lu, Z. Chen, Y. F. Li, et al. Determination of Mercury(II) by Fluorescence Using Deoxyribonucleic Acid Stabilized Silver Nanoclusters. Anal. Lett. 48. 2 (2015). doi: 10.1080/00032719.2014.940527
[27] J. H. Geng, C. Yao, X. H. Kou, et al. A Fluorescent Biofunctional DNA Hydrogel Prepared by Enzymatic Polymerization. Advanced Healthcare Materials. 7. 5 (2018). doi: 10.1002/adhm.201700998
[28] Y. Y. Wang, S. S. Wang, C. S. Lu, et al. Three kinds of DNA-directed nanoclusters cooperating with graphene oxide for assaying mucin 1, carcinoembryonic antigen and cancer antigen 125. Sens. Actuator B-Chem. 262. (2018). doi: 10.1016/j.snb.2018.01.235
[29] H. Oraby, M. M. Senna, M. Elsayed, et al. Fabrication of reverse-osmosis membranes for the desalination of underground water via the gamma-radiation grafting of acrylic acid onto polyethylene films. J Appl Polym Sci. 134. 41 (2017). doi: 10.1002/app.45410
[30] F. X. Sha, G. J. Cheng, Z. Y. Xuan, et al. Free-radical evolution and decay in cross-linked polytetrafluoroethylene irradiated by gamma-rays. Nucl Sci Tech. 33. 5 (2022). doi: 10.1007/s41365-022-01039-5
[31] F. Wang, Q. F. Wu, Y. R. Jiang, et al. Effect of irradiation on temperature performance of dispersion-compensation no-core cascade optical-fiber sensor coated with polydimethylsiloxane film. Nucl Sci Tech. 33. 9 (2022). doi: 10.1007/s41365-

022-01100-3
[32] W. Liu and Y. Yu. Removal of recalcitrant trivalent chromium complexes from industrial wastewater under strict discharge standards. Environmental Technology & Innovation. 23. (2021). doi: 10.1016/j.eti.2021.101644
[33] R. BENCHEIKH-LATMANI, A. OBRAZTSOVA, M. R. MACKEY, et al. Toxicity of Cr(III) to Shewanella sp. Strain MR-4 during Cr(VI) Reduction. Environ. Sci. Technol. 41. 41 (2007). doi: 10.1021/es0622655
[34] M. Chen, Y. Liu, H. Cao, et al. The secondary and aggregation structural changes of BSA induced by trivalent chromium: A biophysical study. Journal of Luminescence. 158. (2015). doi: 10.1016/j.jlumin.2014.09.021
[35] J. Wang, N. Graham, K. Sun, et al. Ultra-low concentrations of detection for fluoride and trivalent chromium ions by multiple biomimetic nanochannels in a PET membrane. Journal of Cleaner Production. 389. (2023). doi: 10.1016/j.jclepro.2023.136055
[36] Y. Ye, H. Liu, L. Yang, et al. Sensitive and selective SERS probe for trivalent chromium detection using citrate attached gold nanoparticles. Nanoscale. 4. 20 (2012). doi: 10.1039/C2NR31985C
[37] S. H. Ren, S. G. Liu, Y. Ling, et al. Fabrication of silver nanoclusters with enhanced fluorescence triggered by ethanol solvent: a selective fluorescent probe for Cr3+ detection. Anal. Bioanal. Chem. 411. 15 (2019). doi: 10.1007/s00216-019-01796-0
[38] K. I. Kim, S. H. Oh, H. D. Kwen, et al. Polymer-copper-modified MWNTs by radiation-induced graft polymerization and their efficient adsorption of odorous gases. J Appl Polym Sci. 126. (2012). doi: 10.1002/app.35453
[39] D. I. Klimov, E. A. Zezina, S. B. Zezin, et al. Radiation-induced preparation of bimetallic nanoparticles in the films of interpolyelectrolyte complexes. Radiat Phys Chem. 142. (2018). doi: 10.1016/j.radphyschem.2017.02.034
[40] J. Y. He, X. Shang, C. L. Yang, et al. Antibody-Responsive Ratiometric Fluorescence Biosensing of Biemissive Silver Nanoclusters Wrapped in Switchable DNA Tweezers. Anal. Chem. 93. 33 (2021). doi: 10.1021/acs.analchem.1c02444
[41] S. Jin, W. Liu, D. Q. Hu, et al. Aggregation-Induced Emission (AIE) in Ag-Au Bimetallic Nanocluster. Chem.-Eur. J. 24. 15 (2018). doi: 10.1002/chem.201800189
[42] M. Ma and S. Zhu. Grafting polyelectrolytes onto polyacrylamide for flocculation - 1. Polymer synthesis and characterization. Colloid and Polymer Science. 277. 2-3 (1999). doi: 10.1007/s003960050375
[43] M. N. Z. Abidin, M. M. Nasef and T. Matsuura. Fouling Prevention in Polymeric Membranes by Radiation Induced Graft Copolymerization. Polymers-Basel. 14. 1 (2022). doi: 10.3390/polym14010197
[44] L. Shang and S. J. Dong. Facile preparation of water-soluble fluorescent silver nanoclusters using a polyelectrolyte template. Chemical Communications. 9 (2008). doi: 10.1039/b717728c
[45] L. G. Wang, X. G. Zhang, S. F. Hou, et al. Preparation and Characterization of Hydrophilic PVDF Membrane via graft modification by Acrylic Acid. Univ Jinan, Jinan, PEOPLES R CHINA. 306-307. (2011). doi: 10.4028/www.scientific.net/AMR.306-307.1563
[46] Y. L. Li, W. Y. Xi, I. Hussain, et al. Facile preparation of silver nanocluster self-assemblies with aggregation-induced emission by equilibrium shifting. Nanoscale. 13. 33 (2021). doi: 10.1039/d1nr03445f
[47] S. A. Cavaco, S. Fernandes, M. M. Quina, et al. Removal of chromium from electroplating industry effluents by ion exchange resins. J Hazard Mater. 144. 3 (2007). doi: 10.1016/j.jhazmat.2007.01.087
[48] M. Chen, H.-H. Cai, F. Yang, et al. Highly sensitive detection of chromium (III) ions by resonance Rayleigh scattering enhanced by gold nanoparticles.

Spectrochimica Acta Part A: Molecular and Biomolecular Spectroscopy. 118. (2014). doi: 10.1016/j.saa.2013.09.058
[49] W.-H. Chen, S.-Y. Lin and C.-Y. Liu. Capillary electrochromatographic separation of metal ion species with on-line detection by inductively coupled plasma mass spectrometry. Analytica Chimica Acta. 410. 1 (2000). doi: 10.1016/S0003-2670(00)00713-3
[50] J. P. Lafleur and E. D. Salin. Speciation of Chromium by High-Performance Thin-Layer Chromatography with Direct Determination by Laser Ablation Inductively Coupled Plasma Mass Spectrometry. Anal. Chem. 80. 17 (2008). doi: 10.1021/ac8010582
[51] J. Threeprom, S. Purachaka and L. Potipan. Simultaneous determination of Cr(III)-EDTA and Cr(VI) by ion interaction chromatography using a C18 column. Journal of Chromatography A. 1073. 1 (2005). doi: 10.1016/j.chroma.2004.09.053
[52] R. M. Cespón-Romero, M. C. Yebra-Biurrun and M. P. Bermejo-Barrera. Preconcentration and speciation of chromium by the determination of total chromium and chromium(III) in natural waters by flame atomic absorption spectrometry with a chelating ion-exchange flow injection system. Analytica Chimica Acta. 327. 1 (1996). doi: 10.1016/0003-2670(96)00062-1